International Journal for Multiscale Computational Engineering, 6(4)281–297(2008)

Wavelet-Based Spatial Scaling of Coupled Reaction-Diffusion Fields

Sudib K. Mishra,[1] *Krishna Muralidharan,*[2] *Pierre A. Deymier*[2] *& George Frantziskonis*[1,2]

[1]*Department of Civil Engineering and Engineering Mechanics*

[2]*Department of Material Science and Engineering, University of Arizona, Tucson, Arizona 85721, USA*

Sreekanth Pannala & Srdjan Simunovic

Computer Science and Mathematics Division, Oak Ridge National Laboratory, Oak Ridge, Tennessee, USA

ABSTRACT

Multiscale schemes for transferring information from fine to coarse scales are typically based on homogenization techniques. Such schemes smooth the fine scale features of the underlying fields, often resulting in the inability to accurately retain the fine scale correlations. In addition, higher-order statistical moments (beyond mean) of the relevant field variables are not necessarily preserved. As a superior alternative to averaging homogenization methods, a wavelet-based scheme for the exchange of information between a reactive and diffusive field in the context of multiscale reaction-diffusion problems is proposed and analyzed. The scheme is shown to be efficient in passing information along scales, from fine to coarse, i.e., upscaling as well as from coarse to fine, i.e., downscaling. It incorporates fine scale statistics (higher-order moments beyond mean), mainly due to the capability of wavelets to represent fields hierarchically. Critical to the success of the scheme is the identification of dominant scales containing the majority of the useful information. The dominant scales in effect specify the coarsest resolution possible. The scheme is applied in detail to the analysis of a diffusive system with a chemically reacting boundary. Reactions are simulated using kinetic Monte Carlo (kMC) and diffusion is solved by finite differences (FDs). Spatial scale differences are present at the interface of the kMC sites and the diffusion grid. The computational efficiency of the scheme is compared to results obtained by averaging homogenization, and to results from a benchmark scheme that ensures spatial scale parity between kMC and FD.

KEYWORDS

multiscaling, spatial scaling, wavelets, reaction-diffusion

*Address all correspondence to frantzis@email.arizona.edu

1. INTRODUCTION

Multiscale methods have become important computational tools in engineering and scientific applications [1–14]. They fall under two general categories, namely, sequential and concurrent. In sequential multiscale techniques, a set of calculations performed at lower scales is used to estimate parameters needed in a model at higher scales [15,16]. In contrast, concurrent multiscale methodologies simultaneously couple different simulation submethods, each at differing levels of scales and accuracy. The more accurate "finer" submethods are usually adaptively invoked [17–19] to selectively model temporal and spatial regions that require a higher-resolution, higher-precision analysis. The exchange of information between the coarser and finer methods occurs via coarse-graining procedures [20–22], where the finer spatial degrees of freedom are lumped together, resulting in fewer coarser spatial degrees of freedom, and thereby enabling the simulations to address larger spatial dimensions and sometimes longer time scales. Typically, in these coarse-graining procedures, upscaling (i.e., from fine to coarse) is performed via a simple or weighted homogenization of the fine-scale data. Consequently, the flow of information in the opposite direction (downscaling) lacks details specific to finer scales.

In this work, a new scheme is proposed that preserves the statistics at all scales to reasonable accuracy and ensures a seamless coupling of coarse and corresponding fine spatial degrees of freedom. Its efficacy as a spatial (up- and down-) scaling tool is demonstrated on a model reaction-diffusion system, given the importance of reaction-diffusion processes in controlling the structure and properties of a wide variety of naturally occurring and man-made materials [23]. The proposed technique is based on wavelets—a multiresolution tool that can hierarchically separate information at different scales and also enable identification of dominant scales of any given signal. The proposed method has some similarities with the heterogeneous multiscale methods (HMMs) [24] in the sense that both provide up- and downscaling capabilities and are flexible enough to include concurrent as well as sequential methods. The use of wavelets in the present method is different from that in [25], where homogenization is achieved by static condensation in scale (as opposed to the usual one, i.e., in space), thus "condensing" the fine scale information. The coupling of the present method with temporal scaling schemes, as discussed throughout the paper, is also a point of differentiation when compared to Ref. 25. However, both methods aim at including the fine scale information during scaling of information.

Solving the problem of diffusion of chemically reactive species efficiently requires a multiscale computational approach capable of combining numerical methods that account for the reaction and diffusion processes. A common way to model diffusion is via application of continuum-level finite differences (or its variations such as finite volumes or finite elements) on the diffusion equation, while an atomistic simulation method is required for an accurate representation of chemical reactions. This implies that mesoscopic or macroscopic dimensions are sufficient for the finite difference diffusion grid, whereas the reaction events have to be handled on a microscopic/submicroscopic scale as illustrated in Fig. 1, which depicts the spatial dimensions of the simulated system required to model species diffusion to and from a reactive surface. The efficient

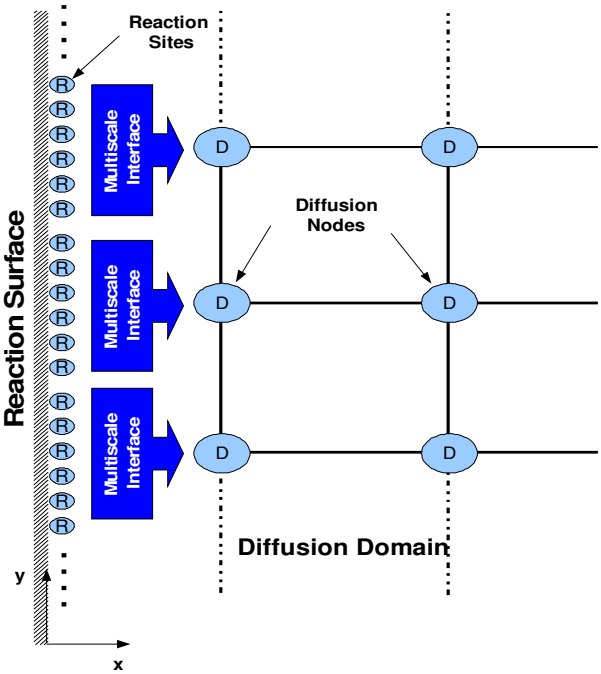

FIGURE 1. Schematic of multiscale interfacing between reactive sites and diffusion grids. R represents the nodes on the reaction grid, D the nodes on diffusion grids

coupling of the methods describing the two processes is thus a challenging proposition since any algorithm adopted must allow for a lossless two-way information exchange pathway between the fine reaction and the coarse diffusion grids; the development of such a method forms the basis of this paper. Furthermore, this work also serves as an important addition to temporal scaling schemes developed by the authors [12–14,26] and offers a spatial scaling procedure that could be used in conjunction with temporal scaling.

2. REACTION-DIFFUSION SYSTEM

A comprehensive as well as an accurate representation of the coupled reaction-diffusion phenomenon requires a microscopic description of both processes. While one could adequately approximate diffusion of chemical species via mesoscale and macroscale continuum representations (finite differences, finite elements), a microscopic representation is still required to accurately account for the reactive processes. Note that the stochastic and microscopic version of the diffusion is also available [27]. Presently, we adopt a deterministic model for diffusion on a macroscopic grid of interest. Thus, a computationally prudent approach would be to couple the microscopic reaction events to the macroscopic continuum representation of diffusion. This would involve a two-way passage of information involving the variation in species concentration that arises due to diffusion and reactions. If one were to restrict the chemically reactive sites to be present only on the surface, as shown in Fig. 1, the coupling of information would only occur between surface reactive sites and diffusion grids.

In this paper, a reaction-diffusion system as shown in Fig. 1 is simulated by using a time-splitting method where the problem is separated into reaction and diffusion subsystems that are coupled through source terms in a segregated fashion. Once the two phenomena are simulated at their characteristic scales, the bridging and exchange of information between the diffusion and reaction systems representing the coarse and fine scales, respectively, is accomplished through a multiscale interface. This section presents the details of the models used for reaction and diffusion processes for the problems herein, while details on the multiscale interface are provided in Sections 3 and 4.

2.1 Simulation of Reactions

The chemical processes are treated under the framework of reaction kinetics. First-order reactions are considered in this work, i.e., the reaction rate is proportional to the concentration of the reactant to its first power. For reversible reactions, such as

$$\begin{aligned} A &\xrightarrow{k_{AB}} B \\ B &\xrightarrow{k_{BA}} A \end{aligned} \tag{1}$$

the first-order rate constants $k_{AB},\ k_{BA}$, each of inverse time units, define the reaction kinetics governed by

$$\begin{aligned} \frac{d[A]}{dt} &= -k_{AB}[A] + k_{BA}[B] \\ \frac{d[B]}{dt} &= -k_{BA}[B] + k_{AB}[A] \end{aligned} \tag{2}$$

The stochastic formulation of Eq. (2) yields a kMC process that is based on the probability distribution function for reaction events [28] expressed in terms of the exponential as follows:

$$P(R = r_i) = 1 - e^{-k[S]\Delta t} \tag{3}$$

where P is the probability of the event r_i . Here, k denotes the reaction rate constant, $[S]$ denotes concentration, and Δt is the event's reaction time demand. Using the time demand, the following equations for forward ($A \rightarrow B$) and backward reaction ($B \rightarrow A$) are obtained:

$$\begin{aligned} t_{AB} &= -\frac{1}{k_{AB}[A]}\ln(1 - R_1) \\ t_{BA} &= -\frac{1}{k_{BA}[B]}\ln(1 - R_2) \end{aligned} \tag{4a}$$

if

$$t_{AB} > t_{BA} \begin{cases} A = A - 1 \\ B = B + 1 \end{cases} \tag{4b}$$

while if

$$t_{BA} > t_{AB} \quad \begin{cases} A = A + 1 \\ B = B - 1 \end{cases} \tag{4c}$$

where R_1 and R_2 are independent random numbers uniformly distributed between zero and unity.

At any particular instant in the simulation, the reaction that occurs is the one that requires the least time [based on Eq. (4a)]. Thus, at every kMC iteration step, two random numbers are generated, i.e., $R_1,\ R_2$ and $t_{AB},\ t_{BA}$ are evaluated based on Eq. (4). The minimum of $t_{AB},\ t_{BA}$ is the time increment associated with the selected reaction event.

2.2 Simulation of Diffusion

The governing equations for the diffusion of species on a 2D, $x-y$ spatial domain is

$$\frac{\partial u\left(x,y,t\right)}{\partial t}=D\left(\frac{\partial^2 u\left(x,y,t\right)}{\partial x^2}+\frac{\partial^2 u\left(x,y,t\right)}{\partial y^2}\right) \quad (5)$$

where D denote the diffusion coefficients, considered constant over the domain, and u denotes concentration of the species. A finite difference explicit Euler scheme, first-order in time and second-order in space, with fixed time steps and fixed spatial discretization is used to solve Eq. (5). The stability criteria for the numerical integration process is guaranteed when the Courant condition is satisfied, i.e.,

$$\Delta t \leq \left[\frac{\left(\Delta s\right)^2}{2D}\right] \quad (6)$$

where $\Delta t,\ \Delta s$ denote the time step and minimum spatial grid size, respectively. In this work, we only consider the deterministic diffusion of species in the 2D domain. The stochastic version of the diffusion process yields a Brownian motion process [27], not examined herein.

As shown in Fig. 1, the spatially 2D model consists of the semi-infinite positive half-space (diffusion domain) with chemical reactions taking place at the boundary of the half-space (reaction domain). At the reactive boundary sites, both A and B are specified by the values evaluated from the reaction kinetics during the operation splitting process. The reflecting boundary condition for the half-space is implemented in the finite difference scheme by setting the outgoing flux to zero. The other end of the discretized diffusion problem in the x direction is sufficiently large so that species do not reach the end within the time frame considered, thus not necessitating an absorbing boundary condition. Finally, periodic boundary conditions are employed for the y direction.

2.3 Scale Disparity in the Reaction-Diffusion System

In the reaction-diffusion model under consideration, the reactive surface is discretized into fine reaction and much coarser diffusion grids. Before every diffusion step, the species concentration at every diffusion site (on the surface) is extracted (via a multiscale interface) from the underlying reaction sites, with the variation in concentration on the reaction sites being dictated by Eq. (4). Between successive diffusion steps, many "inner" reaction steps are carried out since typically the size of a reaction step (4) is much smaller than the diffusion time step size as allowed by the Courant's condition (6). At the end of a diffusion step, the resultant concentration on the surface diffusion sites are then redistributed to the surface reaction sites, once again via the multiscale interface; an illustrative description of the above algorithm is given in the block diagram of Fig. 2.

The optimal number of inner reaction steps (n_r) between successive diffusion steps can be estimated based on the ratio of the characteristic diffusion time T_D and reaction time T_R. There are several ways to

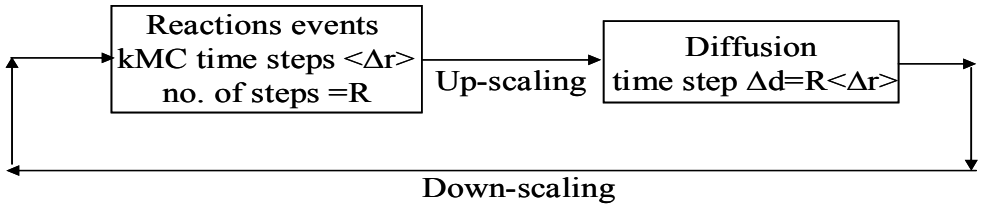

FIGURE 2. Block diagram of the multiscale scheme

estimate T_D, and one of them results in $T_D = 1/\lambda_1$, where λ_1 denotes the smallest eigenvalue of the diffusion tensor [29]. Another way to estimate T_D is based on Eq. (5) and given as

$$T_D = \left(D \left(\frac{1}{L_x^2} + \frac{1}{L_y^2} \right) \right)^{-1} \quad (7)$$

where the spatial discretization scales are denoted by L_x and L_y.

T_R can be estimated based on the fact that in kMC simulations, reaction events are uncorrelated and mutually exclusive. Therefore, the probability of occurrence of reaction r_i out of n possible reaction events is given by

$$P(r_1 \cup r_2 .... \cup r_n) = P(r_1) + P(r_2) + ...P(r_n) \quad (8)$$

where the probability of occurrence of an individual reaction is expressed as

$$P(r_i) = 1 - e^{-k\delta t} \quad (9)$$

Here, k represents the reaction rate constant, and δt is the reaction time associated with reaction r_i. Combining Eqs. (8) and (9), the characteristic reaction time T_D can be obtained from

$$T_R = -\frac{1}{k} \ln \left[1 - \sum_{i=1}^{t} \sum_{j=1}^{r} p_{i,j} \right] \quad (10)$$

where $p_{i,j}$ is the probability of occurrence of a reaction event at site j and at time instant i of the inner kMC steps. In addition to these conditions, the Courant stability condition imposes another bound on the maximum permissible diffusion time step. Presently, we allowed the number of inner reaction steps to be the same as the number of reactive sites. This can be justified from the fact that the occurrence of reaction events are equally likely over any site, and with these many steps it is likely that all the sites will react with a uniform change in concentration profile. Uniformity of this profile is crucial for identification of the dominant scale as discussed in the relevant section.

3. MULTISCALE INTERFACING

The role of the multiscale interface is vital to the reaction-diffusion model under study because it has to ensure that the upscaling of fine scale reaction site concentrations onto coarser scale diffusion sites and the corresponding downscaling (i.e., coupling diffusion grid concentrations to reaction grid concentrations) are performed effectively. In this section we discuss two methods that serve as "multiscale interface," namely, (i) the averaging homogenization scheme and (ii) the wavelet-based spatial scaling scheme. The relative efficacy of the respective methods are discussed in detail in the Results section.

3.1 Homogenization Scheme

For the homogenization scheme, at every diffusion step the concentration at each diffusion node along the reactive boundary is taken to equal the average of the reactive site concentrations in its vicinity. Conversely, at the end of the diffusion step, the resultant concentration at each diffusion node is taken to be representative of all the reactive sites in its vicinity.

3.1.1 Upscaling from Reaction to Diffusion Grid

The upscaling process maps the reaction sites to the surface diffusion grid; since the reaction and diffusion characteristic times are very different, the reactions are allowed to occur for n_r time steps, before upscaling occurs. Mathematically, upscaling can be represented as follows:

$$\{D\}_d^t = [H]_{d,r} \{R\}_r^t \quad (11)$$

where $\{D\}$ and $\{R\}$ represent the diffusion and reaction grids, respectively, with superscript t denoting evaluation at time t, and subscripts d and r denoting the number of surface diffusion grids and reaction sites, respectively, and $[H]$ is a circulant matrix of dimensions [r,d], expressed as

$$[H] = \begin{bmatrix} c_i & c_{i+1} & c_{i+2} & 0 & 0 & 0 & 0 & 0 & c_{i-2} & c_{i-1} \\ c_{i-1} & c_i & c_{i+1} & c_{i+2} & 0 & 0 & 0 & 0 & 0 & c_{i-2} \\ 0 & 0 & 0 & ... & ... & ... & 0 & 0 & 0 & 0 \\ c_{i+2} & 0 & 0 & 0 & 0 & 0 & c_{i-2} & c_{i-1} & c_i & c_{i+1} \\ c_{i+1} & c_{i+2} & 0 & 0 & 0 & 0 & 0 & c_{i-2} & c_{i-1} & c_i \end{bmatrix}_{d,r} \tag{12}$$

The entries in H represent appropriate weights for evaluating the mean field. The present case uses an eight-point stencil for the homogenization operation, while in general the coefficient and indices can be written in a different form [30].

In a way, H acts as a multiscale transfer matrix, and this will become more evident when we introduce the wavelet-based spatial mapping. The deviators from the local mean field at the reaction sites are expressed as

$$\{\delta\}_r = \{R\}_r - [M]_{r,d}\{D\}_d = \{R\}_r - [M]_{r,d}[H]_{d,r}\{R\}_r \tag{13}$$

where matrix M maps the d diffusion grid nodes along the reactive boundary to the r reactive sites, and has the following form:

$$[M] = \begin{bmatrix} [m]_1 & [m]_2 & ..... & [m]_r \end{bmatrix}^T_{d,r}$$

and the submatrices $[m_i]$ comprising the $[M]$ matrix are expressed as

$$[m]_{r/d,d} = \begin{bmatrix} 1 & 0 & 0 & .. & 0 \\ 1 & 0 & 0 & .. & 0 \\ 1 & 0 & 0 & .. & 0 \\ .. & .. & .. & .. & .. \\ 1 & 0 & 0 & .. & 0 \end{bmatrix}_{r/d,d} \tag{14}$$

Thus, the species concentration at any location can be decomposed into a mean field, which is transferred to the coarse scales, i.e., to the diffusion grid, and the residual part, which contains the correlation structure among the individual sites. However, for a deterministic reactive boundary, there is no site-to-site variation in reactions leading to a null residual vector. The mean field in this case is the only contributing part to the reactions and the deterministic system should thus behave as if there is no spatial scaling. This fact is used later for validating the implementations.

3.1.2 Downscaling from Diffusion Grids to Reactive Sites

At the end of a diffusion time step, the species concentrations as they appear on the diffusion grid need to be mapped back onto the reactive sites. This step, crucial to the success of the simulation, is called downscaling (not to be confused to "upsampling," which is a terminology used mostly in signal processing) or backward feedback from the diffusion grid to the reaction sites. Within the homogenization framework, this is done by first assigning the updated mean field of concentrations from the diffusion grid to its contributing reactive sites. This operation is expressed as

$$\{R\}_r^{t+1} = [M]_{r,d}^t \{D\}_d^t \tag{15}$$

where superscript $t+1$ indicates the next diffusion time step after time t. Through downscaling operations on Eq. (15), we essentially assign the individual concentrations of the diffusion grid at time $t+1$ back to its contributing reactive sites. The downscaled reactive concentration profile will have a comparatively smoother profile due to the lack $\{\delta\}_r$ which results from reactive noise. These fluctuations are damped out in homogenization operations. This is shown in the scaled concentration profiles in the Results section.

3.2 Multiscale Interface Using Wavelets

3.2.1 Wavelets and the Wavelet Transform

The wavelet transform is nowadays well established as an important multiresolution mathematical tool [31]. The wavelets are derived from basic templates by scaling and shifting base ("mother") wavelets. A variety of different wavelet transforms exists, and choosing an appropriate wavelet family for a specific problem is, in many respects, similar to choosing an appropriate element for a finite element numerical solution process. The major advantage of wavelet analysis of a function is that it enables

one to extract and examine its features on different scales and locations.

In one dimension, a continuous wavelet $\psi(x)$ transforms a fluctuating function $f(x)$ [31] as

$$W_f(a,b) = \int_{-\infty}^{\infty} f(x)\,\psi_{a,b}(x)\,dx \tag{16}$$

The two-parameter family of functions, $\psi_{a,b}(x) = (1/\sqrt{a})\psi[(x-b)/a]$, is obtained from a single function, ψ, called the mother wavelet, through dilatations by the scaling factor a and translations by the factor b. The factor $1/\sqrt{a}$ is included for normalization. The parameter a can take any positive real value, and the fluctuations of $f(x)$ at position b are measured at the scale a. Given the wavelet coefficients $W_f(a,b)$ associated with a function $f(x)$, it is possible to reconstruct f at a range of scales for x between s_1 and s_2 $(s_1 \le s_2)$ through the inversion formula

$$f_{s_1,s_2}(x) = \frac{1}{c_\psi}\int_{s_1}^{s_2}\int_{-\infty}^{\infty} W_f(a,b)\,\psi_{a,b}(x)\;db\,\frac{da}{a^2} \tag{17}$$

where c_ψ is a constant evaluated from the properties of the wavelet basis. In the limiting case, $s_1 \to 0$ and $s_2 \to \infty$, the original function f is obtained through Eq. (17). When discretized, wavelet analysis can be performed with fast $O(N)$ algorithms as compared to $O[N\log_2(N)]$ for fast Fourier transforms (FFTs). In this work, a biorthogonal spline was used as the mother wavelet, of order (10,4), which preserves symmetry and orthogonality of the dual basis (biorthogonality).

3.2.2 Multiscale Wavelet Interface

The ability of wavelets to hierarchically separate scale-specific details allows the wavelet-based interface to be an effective multiscale tool. Specifically, the wavelet interface allows the separation of coarse and fine-scale spatial fluctuations corresponding to reaction site concentrations, and thereby enables the coarse graining of relevant information during upscaling as well as fine graining during downscaling.

3.2.3 Upscaling from Reaction to Diffusion Grid and Diffusion in the Wavelet Domain

In a fashion analogous to the homogenization scheme, the concentration at the reactive sites represented through vector $\{R\}_r$ can be upscaled to the diffusion grid nodes, thus yielding vector$\{D\}_d$. Let $W_R(s,y)$ denote the wavelet transform of$\{R\}_r$, expressed in terms of scale s and spatial coordinate y. $W_R(s,y)$ is decomposed as

$$\begin{aligned} W_R(s,y) = f_R(s_0,\Delta y) \oplus f_R(s_1,\Delta y) \oplus f_R\left(s_2, 2^1\Delta y\right) \\ \oplus \ldots \oplus f_R\left(s_n, 2^{n-1}\Delta y\right) \end{aligned} \tag{18}$$

where $\oplus$ implies scalewise association in the wavelet analysis formality, $f_R\left(s_i, 2^{i-1}\Delta y\right)$, $i = 1,..,n$ denote the wavelet transform at scale s_i, and sampling interval $2^{i-1}\Delta y$ and $f_R(s_0,\Delta y)$ denotes the transform at the coarsest scale using the scaling function. It should be noted that for vector $\{R\}_r$ of length r, there are $n = \log_2 r - 2$ number of scales (or scale decompositions) available.

Although $n = \log_2 r - 2$ scale decompositions of $\{R\}_r$ are possible, the number of relevant and useful decompositions are restricted by the coarser spatial resolution of the diffusion grid $\{D\}_d$. For example, if there are d number of points in the diffusion grid, then out of $n = \log_2 r - 2^2$ available reaction site scales, only $m = \log_2 d - 2$ scales can be used in upscaling. Thus, the wavelet transform of $\{D\}_d$, $W_R(s,y)$ can be restricted to m scales as

$$\begin{aligned} W_D(s,y) = f_R(s_0,\Delta y) \oplus f_R(s_1,\Delta y) \oplus f_R\left(s_2, 2^1\Delta y\right) \\ \oplus \ldots \oplus f_R\left(s_m, 2^{m-1}\Delta y\right) \end{aligned} \tag{19}$$

It should be noted that for an accurate representation, m should be greater than or equal to a certain number of critical or dominant scales in order to ensure that the energy norm as well as the basic correlation structure of $\{R\}_r$ is essentially preserved during upscaling. The identification of these dominant scales can be accomplished based on the L2-norm of the wavelet coefficients at each scale, with the dominant scales being the ones that contribute significantly toward the total energy (sum over all scale energies). Furthermore, the choice of the inner time steps n_r becomes crucial to the upscaling procedure; ideally, the inner kMC loop should proceed until a

statistically reasonable spatial concentration profile is allowed to develop. Specific details for the identification of dominant scales and the choice of n_r as relevant to the system under study are discussed in the Results section.

With the species concentration upscaled from the reaction sites to the diffusion grid, it is convenient and efficient to solve the diffusion equations in the wavelet domain until the next, i.e., downscaling, step, given that the wavelet transform is linear. Since the scales are only bridged along the y coordinate, the diffusion Eq. (5) is solved in the wavelet domain along this coordinate and subsequently back-transformed at the end of the diffusion step, while the diffusion equation along the x coordinate is always solved in real space, i.e.,

$$\frac{\partial W_y[u(x,y,t)]}{\partial t} = D\left[\frac{\partial^2 W_y[u\,(x,y,t)]}{\partial x^2} + \frac{\partial^2 W_y[u\,(x,y,t)]}{\partial y^2}\right] \tag{20}$$

where W_y denotes the wavelet transform of species concentration u in the y direction only. Equation (20) can be written as

$$\frac{\partial u(x,W_y,t)}{\partial t} = D\left[\frac{\partial^2 u(x,W_y,t)}{\partial x^2} + \frac{\partial^2 u(x,W_y,t)}{\partial y^2}\right] \tag{21}$$

thus expressing u as a function of x, t, and the wavelet transform coordinate y. The inverse wavelet transforms yields u in the x, y, t domain, i.e.,

$$u\,(x,y,t) = W_y^{-1}\left[u(x,W_y,t)\right] \tag{22}$$

3.2.4 Downscaling from Diffusion to Reaction Grid

After the diffusion step, $\{D\}_d$ is downscaled to $\{R\}_r$ thus providing feedback to the reaction sites from the diffusion grid. The wavelet transform of $\{D\}_d$ expressed in Eq. (19) contains $m = \log_2 d - 2$ scales, while $n = \log_2 r - 2$ scales are required to define the wavelet transform of$\{R\}_r$. Since $n > m$, the information in the "missing" scales, i.e., the finer ones, is obtained from the previous time step. This process invokes quasi-stationary approximation where we assume that the fine-scale fluctuations of the concentrations are invariant over the small time steps of integration. As pointed out before, if m is greater than or equal to number of the dominant scales, this is a reasonable assumption that does not introduce measurable error. Then, after downscaling, the wavelet transform of $\{R\}_r$ is expressed as

$$\begin{aligned} W_R(s,y) = {} & f_R(s_0,\Delta y) \oplus f_R(s_1,\Delta y) \oplus f_R\left(s_2, 2^1\Delta y\right) \\ & \oplus ... \oplus f_R\left(s_m, 2^{m-1}\Delta y\right) \oplus \\ & f_R^{-\Delta t}\left(s_{m+1}, 2^m\Delta y\right) \oplus ... \oplus f_R^{-\Delta t}\left(s_n, 2^{n-1}\Delta y\right) \end{aligned} \tag{23}$$

where superscript $-\Delta t$ denotes evaluation at the previous time step. The inverse wavelet transforms yields $\{R\}_r$ in the physical domain that become the initial conditions for the next set of inner kMC steps.

For the problems addressed here, as shown in Fig. 3, the three coarsest scales contain all the dominant information on a coarse grid. In these plots, the wavelet transform coefficients are arranged sequentially, from coarse to fine scales, along the horizontal axes. The concentrations were obtained using the benchmark scheme having the same resolution on diffusion grids and reaction sites. Plots such as Fig. 3 help in selecting an optimal grid for the diffusion and this can be used to develop adaptive methods for solving the diffusion problem efficiently. An estimate of dominant scales can be postulated as

$$\eta = \frac{\sum_{i=1}^{m} E_i}{E} \tag{24}$$

where η is the fractional energy index, E_i is the energy contained in the ith scale, and m is the number of scales considered. The so-called energy in this case is based on the L2-norm. Figure 4 shows the plot of η versus m. It is obvious from the plot that out of all the scales, only the three initial coarsest scales contain more than 99% of the energy. This particular property of wavelet transform is the key to upscaling and helps to retain most significant information of the relevant field in its upscaled version.

4. RESULTS

4.1 Homogenization, Wavelet, and Benchmark

Let $\{R\}_r$ denote the spatial "signal" or vector of concentrations along r number of discrete equidistantly spaced reactive points, $x_1, x_2, ..., x_r$. Simi-

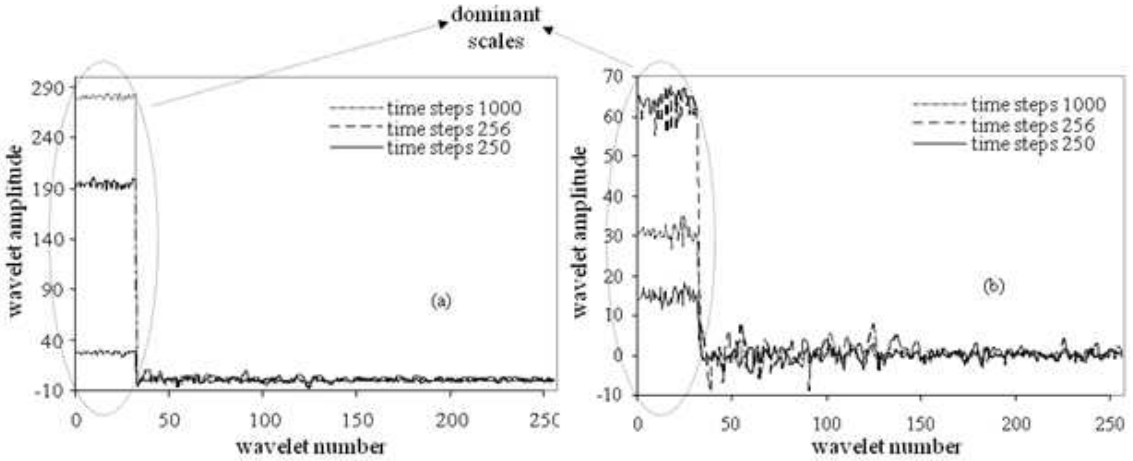

FIGURE 3. Wavelet decomposition of spatial concentration profile and dominant scales for **(a)** species A **(b)** species B

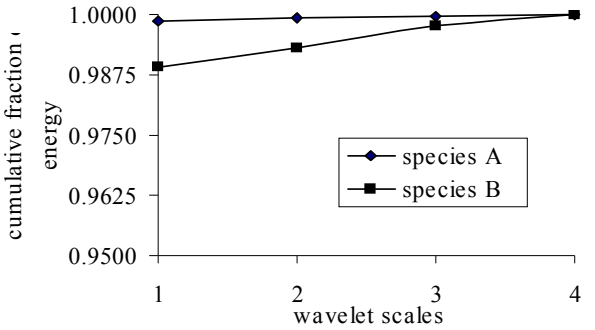

FIGURE 4. Fractions of cumulative energy contained along wavelet scales

larly, let $\{D\}_d$ denote the spatial "signal" of concentrations along d discrete equidistantly spaced diffusion nodes, $x_1, x_2, ..., x_d$, along the reactive boundary. For a benchmark solution of the reaction-diffusion problem $r = d$; in this benchmark solution, no spatial scaling is required, yet the process is computationally cumbersome. For an efficient solution, however, $d < r$; thus, the number of diffusion grid nodes along the reactive boundary are less than the number of reaction sites. This is examined within the context of homogenized and wavelet-based mapping in the following sections.

The homogenized, wavelet based, and benchmark schemes parameters are listed in Table 1 as illustrated in Fig. 1. Of the three, the benchmark scheme is the most accurate, albeit the most computationally expensive, because the diffusion domain discretization is at the scale of the reaction sites. The wavelet-based scheme maps 256 reaction sites to 32 nodes in the diffusion grid, thus there are eight reactive sites contributing to each node in the diffusion domain. The homogenization scheme maps 256 reaction sites to 32 nodes in the diffusion grid.

Isotropic diffusion is considered with a diffusion coefficient $D = 0.05$ space units/s^2. The reaction rate for both forward ($A \rightarrow B$) and backward ($B \rightarrow A$) reactions is considered the same, 2.5/s. Thus, the reaction kinetics are solely governed by the reactive species concentration and will initially be in the direction of lower species concentration. The initial concentration of species A is 100 units and of B is 10 units at the reactive boundary, while away from the boundary (diffusion domain) the initial concentrations are zero.

In the following, the three multiscaling schemes will be compared on the example defined in Table 1. Before proceeding to present any results, it is important to check for species conservation. Conservation is one necessary condition that must be satisfied for any multiscale scheme. We check the mass conservation through counting the total number of species present in the system in kinetic evolution time steps. The upscaled and downscaled concentration profile on the diffusion grid and reaction sites is also shown in Fig. 5. The difference between the homogenization and wavelet-based schemes is obvious form the plot. The proximity of the wavelet-based downscaled reactive profile to the benchmark one is obvious. But this is not the case for the homogenization scheme. The stochasticity is absent

TABLE 1. Discretization Used in the Three Schemes

Models	Diffusion domain				Reaction sites	
	Number of nodes along x	Number of nodes along y, d	Discretization along x	Discretization along y	Number of reaction sites, r	Discretization along x
Benchmark	64	256	0.125 units	0.1250 units	256	0.125 units
Wavelet scheme	64	32	0.125 units	1.0282 units	256	0.125 units
Homogenization scheme	64	32	0.125 units	1.0282 units	256	0.125 units

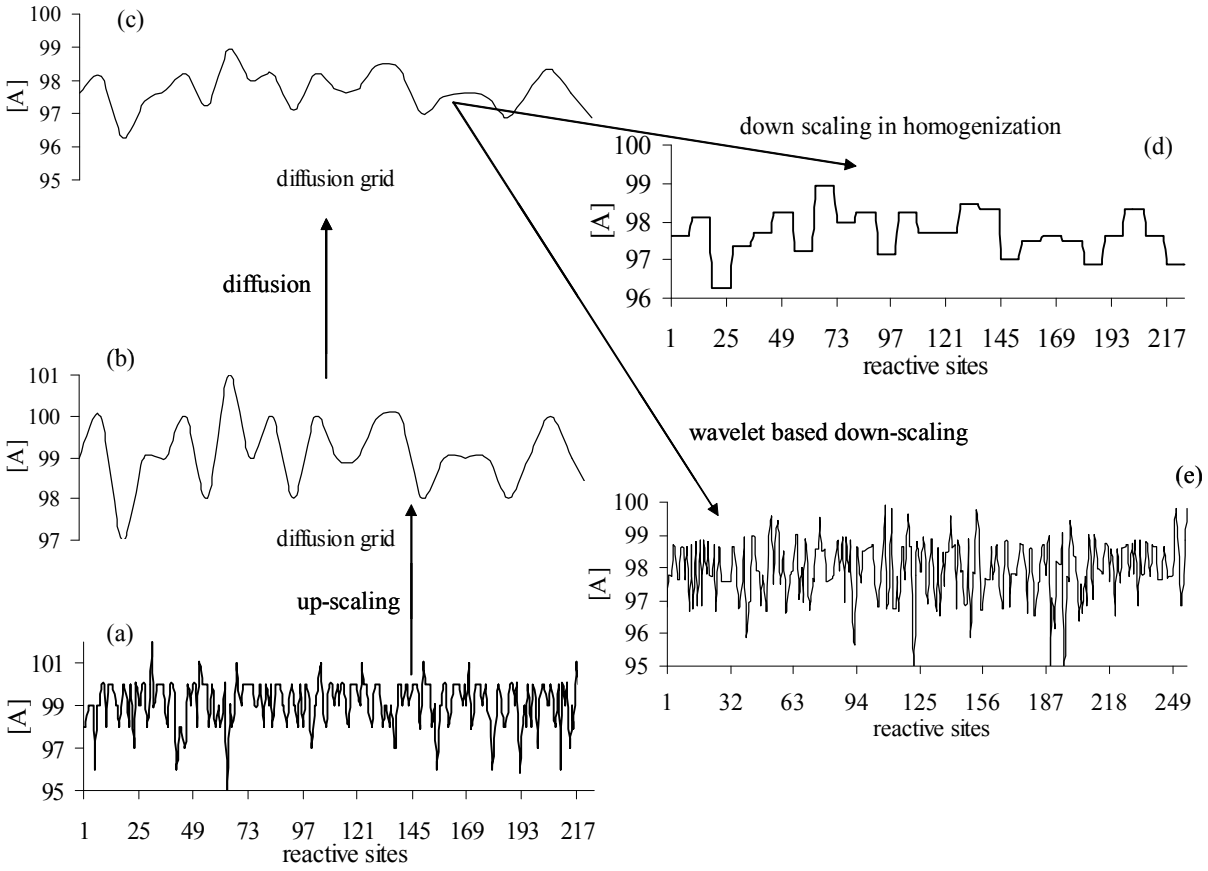

FIGURE 5. Illustration of upscaling and downscaling operations after 256 time steps; **(a)** spatial concentration profile over reactive grid, **(b)** upscaled concentration profile on diffusion grid, **(c)** diffused concentration profile over diffusion grid, **(d)** downscaled spatial concentration profile over reactive sites using the classical homogenization scheme, and **(e)** downscaled spatial concentration profile from the wavelet-based scheme

in the homogenized downscaled profile whereas it is present in the wavelet-based downscaled profile. This is due to the multiresolution capabilities of the wavelet transform and perseverance of correlation in the transformed data.

The parameters listed in Table 1 are used for three different schemes, i.e., the benchmark, the wavelet, and the homogenization. The schemes are allowed to evolve over time. The kinetic evolutions of the species are shown in Fig. 6 for species B.

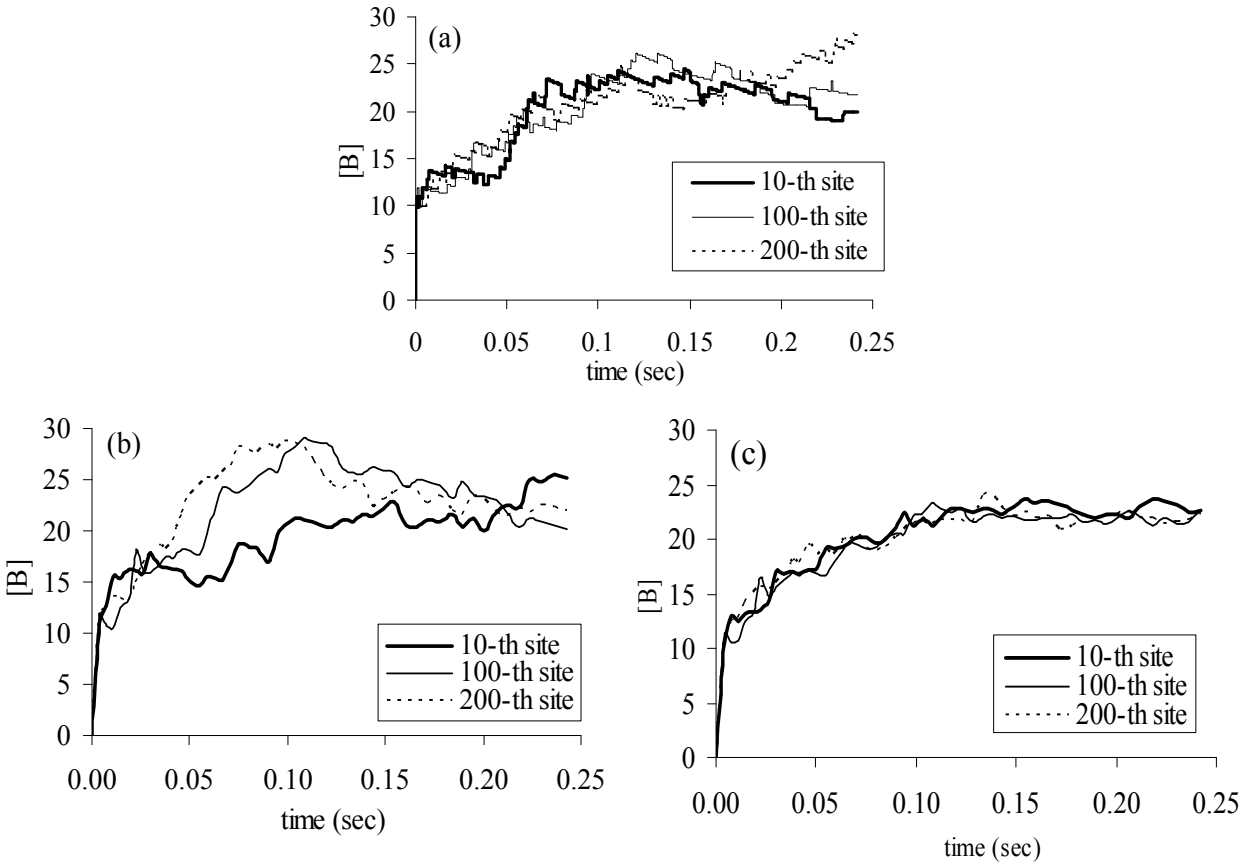

FIGURE 6. The kinetic evolution of species B for **(a)** benchmark, **(b)** wavelet multiscale, and **(c)** homogenization scheme

The benchmark evolution contains significant stochasticity, as dictated by the reactions. The fluctuations are distributed within a concentration band (B between 20 to 30 units) after time 0.1 s. In addition, there are other smaller fluctuations localized in the benchmark evolution. For the homogenization scheme, we see the fluctuations are drastically diminished and all three evolutions in time after 0.1 s tend toward B in the vicinity of 25 units. This is because the homogenization operations smeared evolutions of all sites into a mean field evolution. The wavelet-based scheme however retains these higher fluctuations and the signals stays between $B = 20$ and $B = 30$, yet very small fluctuations seen in the benchmark evolution are not captured due to truncation of higher wavelet scales. However, the ability of the wavelet scheme in retaining a larger portion of the stochasticity is obvious.

From Table 2, it is seen that all three schemes show obvious fluctuations in the kinetic evolution of species, which is due to the kMC reaction process. However, the fluctuations in both the wavelet and homogenization schemes are reduced, as compared to the benchmark scheme. One reason for this is the inner time steps. Another reason for the wavelet scheme fluctuations is that by only considering the dominant scales in the wavelet transform, small scale fluctuations are smeared out. Such smearing is more pronounced in the homogenization scheme since, even though it is incapable of recognizing dominant information, each homogenization yields a spatially flat reaction field.

A clearer view of the kinetic evolution from individual schemes can be derived from the statistical moments associated with the concentrations profiles sampled at various scaled versions. The mo-

TABLE 2. The comparison of statistics (at 256 time steps) from all the schemes, namely, benchmark, wavelet, and homogenization. There are 256 reactive sites and on its upscaled version, the number of sites over which the profile is sampled is 32. On downscaling, the number gets back to 256. Statistics up to fourth order are considered. Same statistics from the various schemes and at different versions of scaling are shown in each single column

Domain	Mean			Standard deviation		
	Benchmark	Wavelet	Homogenized	Benchmark	Wavelet	Homogenized
Reaction grid	99.1877	99.1875	99.1875	0.9395	0.9393	0.9393
Upscaled	99.1877	99.1874	99.2125	0.9395	0.9072	0.8206
Diffusion grid	98.1243	98.1237	98.2465	0.9238	0.9035	0.8632
Downscaled	98.1243	98.1237	98.2465	0.9238	0.9381	0.8630
Domain	Skewness			Kurtosis		
Reaction grid	-0.7815	-0.7832	-0.7832	0.4095	0.4165	0.4165
Upscaled	-0.7815	-0.6985	-0.5223	0.4095	0.3495	0.2867
Diffusion grid	-0.5815	-0.5635	-0.5227	0.4094	0.3496	0.2448
Downscaled	-0.5815	-0.6035	-0.5222	0.4094	0.4164	0.0507

ments up to fourth order were calculated and compared for various versions of the scaled concentration profiles. The comparisons are shown in Table 2. Note that the statistics pertain to species concentrations along adjacent reactive-diffusive sites. These results show the efficacy of the wavelet scheme in retaining higher-order moments in comparison to the classical homogenization scheme. The efficiency of the multiscale schemes depends on their capability to accurately retain temporal as well as spatial information on the concentrations. Thus, along with the temporal evolution, the spatial distribution of concentrations should be studied; typical spatial maps, at a particular time, are shown in Fig. 7.

As expected, both the homogenized and wavelet spatial scaling schemes compromise to some extent in representing the fine scale fluctuations for the gain in computational efficiency. However, it is shown in the sequence that the wavelet scheme provides superior information as compared to the homogenized scheme. The statistics of the kinetic evolution signals are well preserved in the wavelet scheme. as has already been seen in Fig. 6. as compared to the homogenization scheme. The deviation in fluctuations along the spatial axis Y between the benchmark and wavelet schemes is due to the exclusion of ultrafine scales in wavelet decomposition. By increasing the number of wavelet scales in up- and downscaling brings increasingly more fluctuations, as shown in Fig. 8. This assures monotonous convergence of the wavelet scheme.

Another very important measure is the capturing of correlation structures by the multiscale schemes. Even though the kMC reactions are uncorrelated, diffusion of species in the y direction introduces correlations. In order to examine whether the multiscale schemes are capable of capturing such correlations, an enhanced correlation on the concentrations along the reactive sites is imposed. Even though these do not contribute to the physics of the problem, they do help understand the effect of multiscaling in detail. Enhanced correlations are achieved by using the ARMA (autoregressive moving average) model. ARMA has proved to be efficient in relevant modeling schemes [33,34].

The ARMA (3, 2) with parameters such that the underlying statistics remain intact is used. Figure 9 shows the spatial autocorrelation of concentrations along the reactive sites (y direction, at x = 0) as it results from the three schemes. The benchmark scheme has the correlation structure since it results from the diffusion processes and the ARMA enhancement. The wavelet scheme is capable of capturing the spatial correlations by including only the first two coarsest scales (i.e., the scales containing the scaling coefficients and the next finer scale containing the coarsest wavelet coefficients). With three (or more) scales, the autocorrelation structure from

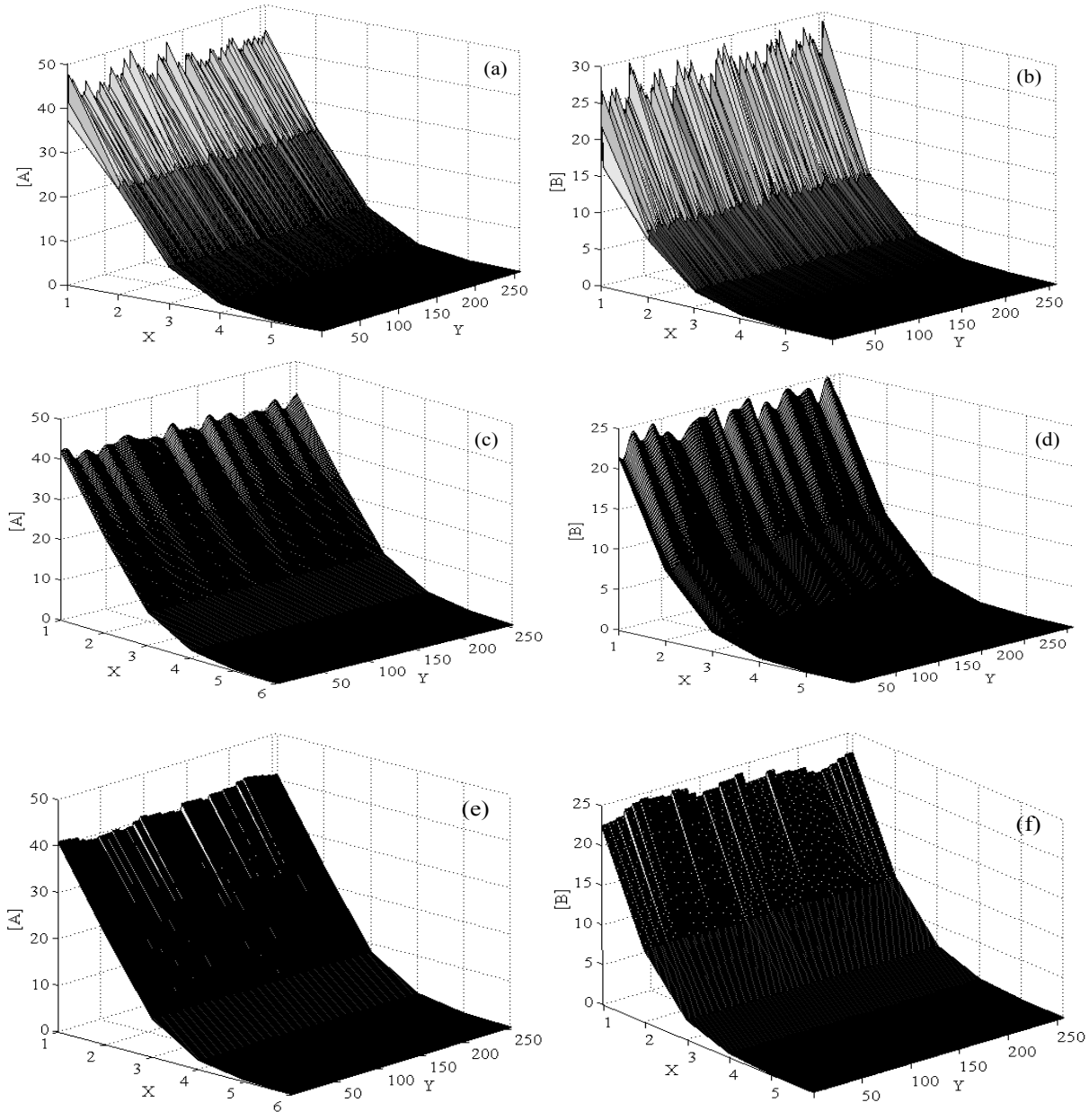

FIGURE 7. The concentration map of **(a)** species A from benchmark scheme, **(b)** species B from benchmark scheme, **(c)** species A from wavelet scheme, **(d)** species B from wavelet scheme, **(e)** species A from homogenized scheme, and **(f)** species B from homogenized scheme. The maps are taken at 12,500 time steps (0.25 s) dictated by kMC

the wavelet scheme is practically identical to the one from the benchmark. To the contrary, the homogenization scheme is incapable of capturing the correlations.

4.2 CPU Time in the Schemes

For the values listed in Table 1, Fig. 10 shows the CPU time needed for each of the three schemes de-

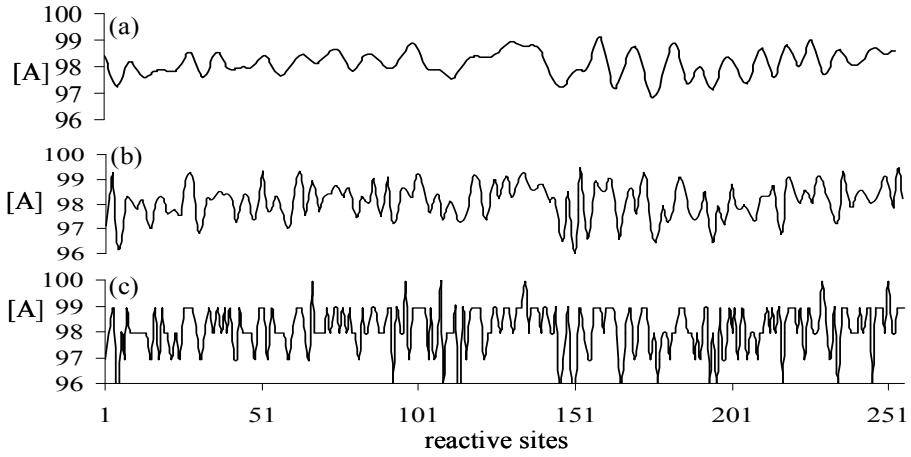

FIGURE 8. The change in downscaled concentration profiles with increasing number of wavelet scales; **(a)** with only one, **(b)** with three, and **(c)** with all five scales

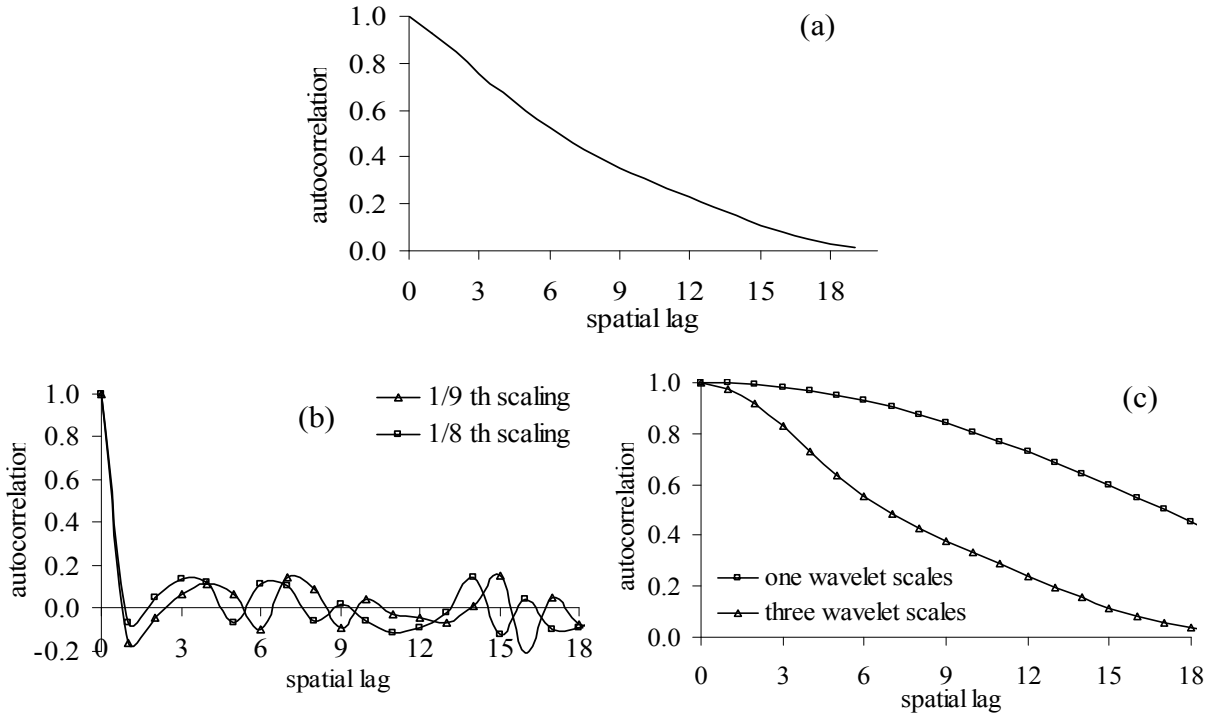

FIGURE 9. The autocorrelation function resulting from **(a)** benchmark, **(b)** homogenization, and **(c)** wavelet scheme. The scaling in the homogenized and wavelet schemes is defined as $S = (\log_2 r / \log_2 d)$ where r is the number of reaction sites and d is the number of diffusion sites

scribed. The large time demand for the benchmark scheme is obvious, as compared to the homogenization scheme, which demands the least CPU time, and the wavelet one, which demands slightly more time than the homogenization one. This little difference in processing time is offset by the reasonable degree of accuracy offered by the wavelet-based scheme.

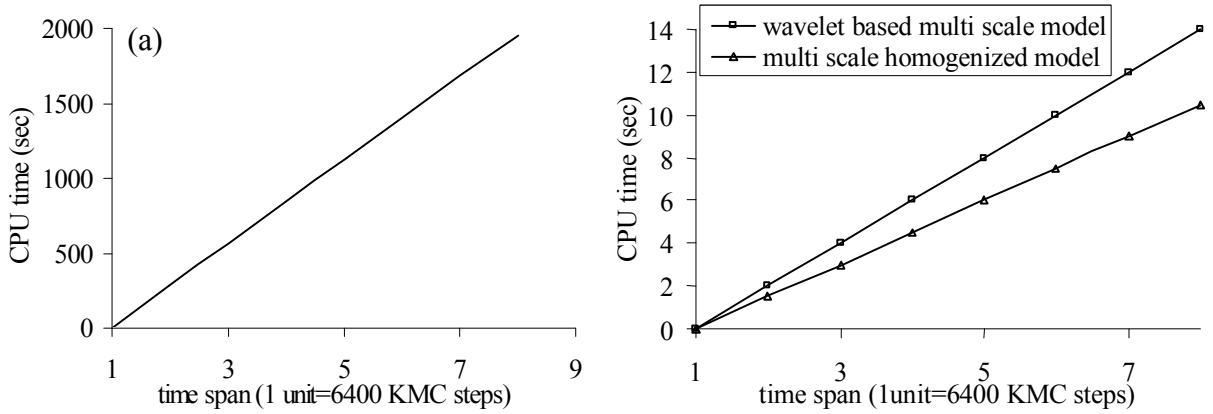

FIGURE 10. The CPU time demand for **(a)** benchmark, **(b)** wavelet, and **(c)** homogenization scheme. These times are for a computer with Intel Pentium IV CPU with 2 GHz clock speed

5. CONCLUSIONS

In this paper, we have proposed a new wavelet-based multiscaling method capable of passing information between spatial scales while preserving the inherent higher-order statistics and correlations structures. The numerous advantages of this method as well as its superiority to homogenization schemes are clearly shown in this work. The spatial scaling wavelet scheme presented herein is offered as a complement to wavelet-based temporal multiscaling presented elsewhere. Even though the spatial multiscaling offers reduced CPU time demand while providing reasonable accuracy, a combined temporal and spatial scaling is required to simulate problems as the present reaction-diffusion system efficiently, i.e., representing the behavior accurately at all spatiotemporal scales. A homogenization scheme may offer a simple alternative to the wavelet one, yet its efficacy is inferior, especially with respect to capturing any spatial correlations, retaining important stochasticity in kinetic evolution, and in preserving the higher-order moments of system parameters that are present in the benchmark system.

ACKNOWLEDGMENTS

This research is sponsored by the Mathematical, Information, and Computational Sciences Division, Office of Advanced Scientific Computing Research, U.S. Department of Energy, with Dr. Sandy Landsberg as the program manager. The work was partly performed at the Oak Ridge National Laboratory, which is managed by UT-Battelle, LLC, under Contract No. De-AC05-00OR22725. Discussions with M. Syamlal, T. J. O'Brien, and D. Alfonso of the National Energy Technology Laboratory (NETL), Stuart Daw of Oak Ridge National Laboratory, and Rodney Fox and Z. Gao of Iowa State University have been very useful.

REFERENCES

1. Vvedensky, D., Multiscale modeling of nanostructures. *J. Phys. Cond. Matter.* **16**:R1537–R1576, 2004.
2. Marin, G. B., ed. Multiscale analysis, in *Advances in Chemical Engineering*, Elsevier, Amsterdam, Netherlands, series 30, 1–309, 2005.
3. Dollet, A., Multiscale modeling of CVD film growth—A review of recent works. *Surf. Coatings Technol.* **177–178**:245–251, 2004.
4. Hsiaotao, T., and Jinghai, L. I., Multiscale Analysis and Modeling of Multiphase Chemical Reactors. *Adv. Powder Technol.* **15**:607–627, 2004.
5. Murthy, J. Y., Narumanchi, S. V. J., Pascual-Gutierrez, J. A., Wang, T., Ni, C., and Mathur, S. R., Review of multiscale simulation in submicron heat transfer. *Int. J. Multiscale Comput. Eng.* **3**:5–31, 2005.
6. Sinha, S., and Goodson, K. E., Review: Multiscale thermal modeling in nanoelectronics. *Int. J. Multiscale Comput. Eng.* **3**:107–133, 2005.

7. Vasenkov, A. V., Fedoseyev, A. I., Kolobov, V. I., Choi, H. S., Hong, K. H., Kim, K., Kim, J., Lee, H. S., and Shin, J. K., Computational framework for modeling of multi-scale processes. *Comput. Theor. Nanosci.* **3**:453–458, 2006.
8. Kevrekidis, I. G., Equation-free coarse-grained multiscale computation: enabling microscopic simulators to perform system-level tasks. *Comm. Math. Sci.* **14**:715–729, 2003.
9. Frantziskonis, G., and Deymier, P. A., Wavelet methods for analyzing and bridging simulations at complementary scales—The compound wavelet matrix and application to microstructure evolution. *Model. Simul. Mater. Sci. Eng.* **8**:649–664, 2000.
10. Frantziskonis, G., and Hansen, A., Wavelet-based multiscaling in self-affine random media. *Fractals.* **8**:403–411, 2000.
11. Frantziskonis, G., Wavelet-based multiscaling—Application to material porosity and identification of dominant scales. *Prob. Eng. Mech.* **17**:349–357, 2002.
12. Frantziskonis, G., and Deymier, P. A., Wavelet-based spatial and temporal multiscaling: bridging the atomistic and continuum space and time scales. *Phys. Rev. B.* **68**:024105, 2003.
13. Muralidharan, K., Deymier, P. A., and Simmons, J. H. A., Concurrent multiscale FDTD-MD method for bridging an elastic continuum to an atomic system. *Modell. Simul. Mater. Sci. Eng.* **11**:487–501, 2003.
14. Muralidharan, K., Mishra, S. K., Frantziskonis, G. F., Deymier, P. A., Nukala, P., Simunovic, S., and Pannala, S., The dynamic compound wavelet method for multiscale/multiphysics simulations. *Phys. Rev. E.* **77**:026714, 2008.
15. Mullins, M., and Dokanish, M. A., Simulation of the (001) plane crack in α-iron employing a new boundary scheme. *Phil. Mag. A.* **46**:771–780, 1982.
16. Tadmor, E. B., Phillips, R., and Ortiz, M., Mixed atomistic and continuum models of deformation in solids. *Langmuir*. **12**:4529–4544, 1996.
17. Deymier, P. A., Oh, K. D., Muralidharan, K., Frantziskonis, G., and Runge, K., Selection of domains for coarse and fine levels of description in mixed-potential systems. *J. Comp-Aided Mater. Des.* **13**:17–44, 2006.
18. Praprotnik, M., DelleSite, L., and Kremer, K., Adaptive resolution molecular-dynamics simulation: changing the degrees of freedom on the fly. *J. Chem. Phys.* **123**:224106, 2005.
19. Abrams, C. J., Concurrent dual-resolution monte-carlo simulation of liquid methane. *J. Chem. Phys.* **123**:234101, 2005.
20. Ensing, B., Nielsen, S. O., Moore, P. B., Klein, M. L., Parrinello, M., Energy conservation in adaptive hybrid atomistic/coarse-grain molecular dynamics. *J. Chem. Theory Comput.* **2**:1100–1105, 2007.
21. Rickman, J. M., and Lesar, R., Issues in the coarse-graining of dislocation energetics and dynamics. *Scripta Mater*. **54**:735–739, 2006.
22. Rudd, R. E., and Broughton, J. Q., Coarse-grained molecular dynamics and the atomic limit of finite elements. *Phys. Rev. B.* **58**:5893–5896, 1998.
23. Grzybowski, B. A., Bishop, K. J. M., Campbell, C. J., Fialkowski, M., and Smoukov, S. K., Micro- and nanotechnology via reaction-diffusion. *Soft Matter.* **1**:114–128, 2005.
24. E, W., and Engquist, B., The heterogeneous multi-scale methods. *Comm. Math. Sci.* **1**:87–132, 2002.
25. Mehraeen, S., and Chen, J. S., Multiscale wavelet-based homogenization of heterogeneous media. *Finite Elements in Analysis and Design*. **40**:1665–1679, 2004.
26. Mishra, S. K., Muralidharan, K., Pannalla, S., Simunovic, S., Daw, S. C., Nukala, P., Fox, R., Deymier, P. A., and Frantziskonis, G., Spatiotemporal compound wavelet matrix framework for multiscale/multiphysics reactor simulation: Case study of a heterogeneous reaction/diffusion system. *Int. J. Chem. Reactor Eng.* **6**:A18, 2008.
27. Gardiner, C. W., *Handbook of Stochastic Methods: For Physics, Chemistry and the Natural Sciences,* 2nd ed. Springer, New York, 1996.
28. Gillespie, D. T., Exact stochastic simulation of coupled chemical reactions. *J. Phys. Chem.* **81**:2340-2361, 1977.
29. Manning, M. R., Characteristic modes of iso-

topic variations in atmospheric chemistry. *Geophys. Res. Lett.* **26**:1263–1266, 1999.

30. Pavliotis, G. A., and Stuart, A. M., *Multiscale Methods: Averaging and Homogenization,* Springer, New York, 2007.
31. Daubechies, I., Mallat, S., and Willsky, A. S., Special Issue on wavelet transforms and multiresolution signal analysis—Introduction. *IEEE Trans. Info. Theory.* **38**:529–531, 1992.
32. Cohen, A., Daubechies, I., Jawerth, B., and Vial, P., Multiresolution analysis, wavelets and fast algorithms on an interval. *Compt. Rend. Acad. Sci. Math.* **316**:417–421, 1993.
33. Na, S. S., and Rhee, H. K., Polynomial ARMA model identification for a continuous styrene polymerization reactor using on-line measurements of polymer properties. *J. Appl. Polym. Sci.* **76**:1889–1901, 2000.
34. Shaojian, S., and Parthasarathy, R., Protein sequence and structure relationship ARMA spectral analysis: Application to membrane proteins. *Biophys. J.* **66**:2092–2106, 1994.